The effect of microsolvation on the structure, nuclear quadrupole coupling and internal rotation: The methyl carbamate···(H$_2$O)$_{1\text{-}3}$ complexes.

Pablo Pinacho,[a,b,*] Juan Carlos López,[a] Zbigniew Kisiel,[c] and Susana Blanco[a,*]

Affiliations

[a] Department of Physical Chemistry and Inorganic Chemistry, IU-CINQUIMA, University of Valladolid, Paseo Belen 7, Valladolid, 47011 Spain.

[b] Department of Physical Chemistry, University of the Basque Country (UPV/EHU), B° Sarriena, S/N, Leioa, 48940, Spain.

[c] Institute of Physics, Polish Academy of Sciences, Al. Lotników 32/46, Warsaw, 02-668, Poland

Authors to whom correspondence should be addressed:

* Pablo Pinacho, pablo.pinacho@ehu.eus

* Susana Blanco, susana.blanco@uva.es

ABSTRACT

Microsolvation of the carbamate moiety delivers precise information on complexation effects on the N-C=O backbone and is of relevance to the peptide bond functionality. In this context, the mono-, di- and trihydrated complexes of methyl carbamate have been studied in a molecular expansion by high-resolution microwave spectroscopy, using chirped-pulse and Fabry-Perot resonator FTMW instruments covering the frequency range from 2 to 18 GHz. From the rotational constants of the parent and the $^{18}O_w$ substituted monoisotopologues, accurate values have been derived for the geometries of the hydrogen bond interactions. The nuclear quadrupole coupling constant χ_{cc} of the nitrogen nucleus provides a direct measure of complexation changes and decreases with the degree of hydration, whereas the hindered internal rotation barrier increases slightly on microsolvation. Both tendencies could have a common origin in the π-cooperative inductive effects as the microsolvation series progresses. All transitions are split by the internal rotation of the methyl top, and the nuclear quadrupole coupling, and in the largest cluster they are additionally split by an inversion motion.

Introduction

The carbamate moiety (-NCO$_2$-) is commonly found in biologically active molecules with pharmacological[1,2] and industrial[3] applications, especially in polyurethane polymer production.[4] A carbamate can be considered as an ester-derivative of an amide and shares the main structural moiety with the peptide bond, the N–C=O group. The peptide bond is responsible for protein formation and plays a crucial role in protein structures, as it is the link between two amino acids.[5] Studying the effects of microhydration at different degrees of hydration of the peptide bond is of great interest for a better knowledge of the associated biological processes, and the role that water plays in them.[6-11] Water is a double hydrogen bond donor/acceptor with the ability to form strong interactions with the peptide linkage. Microsolvated clusters of increasing complexity can provide valuable information on the way water clusters associate with biomolecules by forming chains or sequential cycles. Carbamates featuring the N–C=O backbone, represent appropriate models to study the peptide bond functionality and its microsolvation behavior. Such complexes can be formed in a supersonic expansion and characterized by high-resolution spectroscopy.

Methyl carbamate (C$_2$H$_5$NO$_2$, mcb) is the simplest representative of this family of compounds and, in addition to its importance in the biological environment, it is believed to be present in the interstellar medium as a precursor of biological molecules. In order to provide an extensive basis for its radio astronomy detection, it was thoroughly studied in the gas phase using IR[12] and microwave spectroscopy in both the ground[13-15] and the lowest vibrationally excited state.[16] Methyl carbamate can exist in two configurations, *syn* or *anti* based on the orientation of the methyl group relative to the carbonyl oxygen (Figure 1). Only the *syn* configuration has so far been reported experimentally, as the *anti*-form is significantly higher in energy according to previous studies.[12-16]
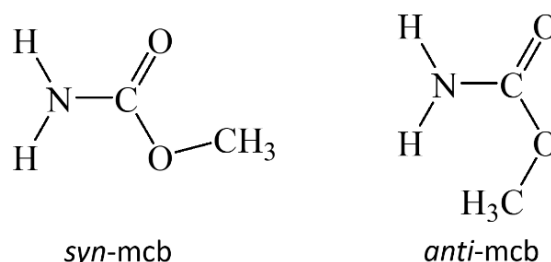

Figure 1. Schematic representation of the *syn* and *anti* configurations for methyl carbamate (mcb).

The microsolvation of the carbamate group in methyl carbamate can provide relevant information about the hydration of a polar substituted peptide linkage in the first steps of solvation. The study of complexes between mcb and water complements previous results of amide-type microsolvated molecules, as formamide,[6,8-10] formanilide,[11] and other members of the carbamate family; such as ethyl carbamate,[17] and butyl carbamate.[18] In this work, we used molecular beam Fourier transform microwave spectroscopy to investigate the complexes of mcb with up to three molecules of water, generated in a supersonic expansion. We investigated the effect of water on the mcb molecular properties, as reflected in changes of the nuclear quadrupole coupling constants (NQCCs) of the ^{14}N nucleus and the internal rotation barrier of the methyl top. Such information is available since the complexes with one or two molecules of water show fine and hyperfine structure on the spectra (Figure 2 a), and b)), arising from the internal rotation of the O-CH$_3$ top, and the presence of the ^{14}N nucleus, respectively. The complex with three molecules of water, presents a further splitting due to an inversion motion (Figure 2 c)), similar to that observed for other trihydrated complexes.[10,17]
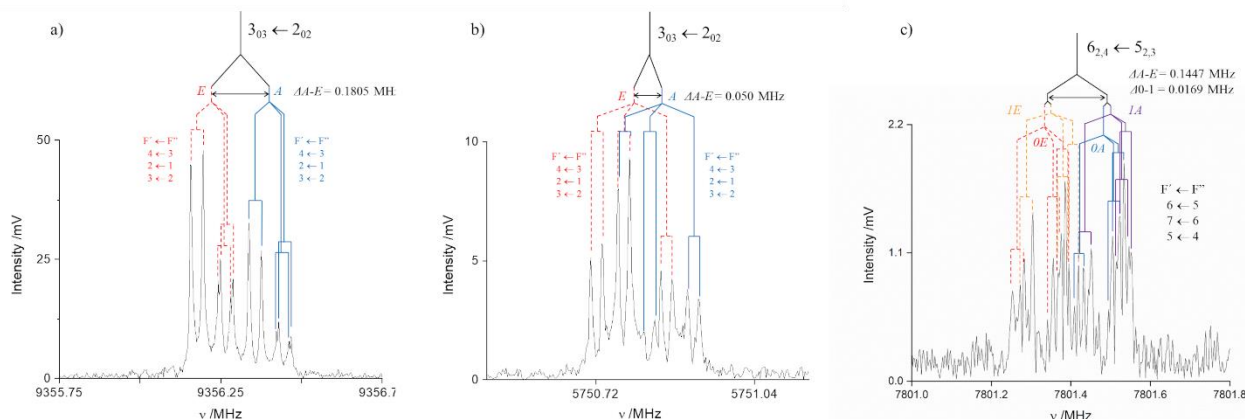
Figure 2. The $3_{0,3} \leftarrow 2_{0,2}$ rotational transition for a) *syn*-mcb-w-a and b) *syn*-mcb-w$_2$-a complexes illustrating the origin of the splitting structures. First, each transition is split by internal rotation into two components, *A* (blue) and *E* (red). Each component further splits due to the nuclear quadrupole coupling (F′ ← F′′ transitions). c) For the *syn*-mcb-w$_3$-a complex the $6_{2,4} \leftarrow 5_{2,3}$ transition is depicted, showing the additional splitting due to the inversion motion into 0 *A* (blue), 0 *E* (red), 1 *A* (purple) and 1 *E* (orange) states. Each transition appears as a doublet because of the instrumental Doppler effect.

Experimental and theoretical methods

Methyl carbamate is a white crystalline solid with melting point of *ca*. 57 °C. It was purchased and used without further purification. The sample was heated to approximately 90 °C in a stainless steel heated pulsed nozzle and mixed with argon or neon as carrier gases. A receptacle containing water was placed in the gas line before the nozzle to provide enough water vapor in the gas phase. It should be noted that mcb is hygroscopic, raising the possibility that water molecules for the complexation could already be present as crystallization water in the sample. A supersonic expansion pulse of 900 μs length was generated by passing the sample mixture, at a backing pressure between 2-3 bar, through the small diameter nozzle (1 mm) into the high-vacuum cavity. This provided the appropriate environment for the generation of complexes and their subsequent study. The microwave spectrum of mcb was initially recorded at frequencies from 2 to 8 GHz using the chirped-pulse Fourier transform spectrometer (CP-FTMW)[19,20] at the University of Valladolid. The spectrometer features a resolution of better than 25 kHz, and the uncertainty in frequency determination is better than 15 kHz. The spectrum was recorded using a sample polarization chirped pulse of *ca*. 4 μs. The Free Induction Decay molecular emission signal was recorded in the time domain for 40 μs and converted into the frequency domain by the application of a fast Fourier transformation. Refined measurements in the 5-12 GHz and in the 8-18 GHz regions were carried out in two Fourier transform microwave spectrometers (FTMW) based on the Balle-Flygare cavity design, one at the University of Valladolid[21] and the other at the Institute of Physics in Warsaw[22,23] respectively. In these instruments, a narrow band of approximately 2 MHz can be recorded in a single step, with transition frequency measurement accuracy better than 3 kHz, allowing for full resolution of the hyperfine structure due to the nuclear quadrupole coupling and the fine structure due to large amplitude motions.

The spectral signal-to-noise ratio was not sufficient for the observation of natural abundance isotopologues. A mixture of H$_2$O and isotopically enriched H$_2$^{18}O (99%) in proportion of 3:1 was used in order to record the rotational spectra of the ^{18}O$_w$ monoisotopically substituted complexes. The rotational constants for the isotopologues were obtained by measuring selected transitions. Complete line lists of observed frequencies for all of the observed species are collected in the supplementary information.

Prior to experiments, quantum chemical calculations were performed using Gaussian 09[24] so as to identify the preferred interaction sites between mcb and water. Different structures were tested for the microsolvated complexes with up to three water molecules, with starting points based on previously reported similar complexes.[6,8-18] The conformational search for the trihydrate was completed using the conformer-rotamer ensemble sampling tool (CREST).[25] The considered geometries were optimized with DFT by using the B3LYP[26] functional combined with Pople´s basis set 6-311++G(d,p)[27] and including vibrational harmonic terms. Grimme´s dispersion correction (D3)[28] was implemented in order to improve the predictions performed by the B3LYP functional, due to its poor description of dispersion forces contributing in cases of long-range interaction such as hydrogen bonds.[29] These were later optimized using B3LYP-D3BJ/6-311++G(2d,p)[30] including the Becke-Johnson damping function.[31] Additional calculations using the MP2 method[32] combined with the 6-311++G(d,p) basis set were performed so as to compare the values of the internal rotation barrier height and the NQCCs. The computed rotational constants, dipole moment components, and NQCCs, were used for predicting the microwave spectra for the complexes. The theoretical internal rotation barrier values and calculated internal rotation parameters were also used in prediction of the anticipated experimental splittings in the transitions.

Different aspects of the hydrogen bond interactions and cooperativity effects were also investigated through Natural Bond Orbital (NBO) computations.[33]

Results and discussion

Conformational search

For the mcb···(H$_2$O)$_1$ complex three different water interaction sites were considered, in analogy to those observed experimentally for formamide.[8] Such complexes could also be formed with both *syn* and *anti* mcb. The optimized geometries for the six possible conformations are presented in Figure S1 in the supplementary material. For the disposition of the water molecules in the mcb···(H$_2$O)$_2$ complex, the same arrangement

2

was considered for both *syn* and *anti* mcb. The structures of the complexes were drawn on the basis of the observed structures for similar complexes in formamide, and ethyl carbamate.[8,17] Their geometries and energies are shown in Figure S2. Similarly, for mcb···(H$_2$O)$_3$, the configuration previously seen in related complexes was considered for both the *syn* and *anti* mcb forms.[10,17] Additional configurations with different orientations for the non-bonded hydrogen atoms in water were included. We extended the conformational search using the CREST tool. The most stable forms for the complex are depicted in Figure S3. In all cases, the complexes with *syn* mcb are much lower in energy than the *anti*-configuration, in similarity to the mcb monomer. The theoretical parameters for the most relevant structures considered in this work are collected in Tables S1-S3.

Syn-methyl carbamate···(H$_2$O)$_{1-3}$ complexes

First identifications of the species present in the supersonic expansion were made from the CP-FTMW spectrum. The rich fine and hyperfine structures were characterized in more detail by recording each transition using the Balle-Flygare spectrometers.

Only a few transitions from the monomer can be found in the 2 – 8 GHz region. After excluding the known lines, several intense lines remained, which were assigned to the lowest energy *syn*-methyl carbamate···(H$_2$O) complex (*syn*-mcb-w-a) on the basis of the good agreement with the spectrum predicted for this species (Table 1). The predicted higher energy conformers for the monohydrated complex have not been identified. As expected, each rotational transition of the *syn*-mcb-w-a cluster appeared as a doublet of equal intensity caused by the interaction of the internal rotation of the methyl group with the overall rotation giving rise to *A* and *E* internal rotation substates. Each transition is further split due to nuclear quadrupole coupling arising from the presence of a ^{14}N nucleus in methyl carbamate with the nuclear spin *I* = 1 (Figure 2 a)). Notably, no further splittings due to tunneling motions in the water molecule were observed. A subsequent set of lines with recognizable a-type patterns and net intensity about 10 times smaller than mcb···(H$_2$O)$_1$ was assigned to the *syn*-methyl carbamate···(H$_2$O)$_2$ complex (*syn*-mcb-w$_2$-a, Table 1).

Table 1. Observed and theoretical (B3LYP-D3BJ/6-311++G(2d,p)) parameters for the *syn*-mcb···(H$_2$O)$_{1-3}$ complexes using XIAM.

| Parameter[a]	*syn*-mcb-w-a Experimental	*syn*-mcb-w-a Theoretical	*syn*-mcb-w$_2$-a Experimental	*syn*-mcb-w$_2$-a Theoretical	*syn*-mcb-w$_3$-a Experimental 0	*syn*-mcb-w$_3$-a Experimental 1	*syn*-mcb-w$_3$-a Theoretical
A /MHz	8056.7763(10)[b]	8072	3819.222(15)	3924	2304.127(16)	2304.384(16)	2331
B /MHz	1707.32152(36)	1728	1083.85140(39)	1098	703.15584(77)	703.16483(76)	722
C /MHz	1423.80887(32)	1442	851.82561(25)	866	552.60742(62)	552.60508(62)	563
Δ_J /kHz	0.4860(55)	0.415	0.1700(21)	0.141	0.2229(26)	0.2253(26)	0.175
Δ_{JK} /kHz	0.785(45)	0.0731	1.086(51)	0.707	-2.089(69)	-1.772(70)	-0.736
Δ_K /kHz	[0][c]	21.5	[0]	4.37	[0]	[0]	6.23
δ_J /kHz	0.1022(53)	0.0745	0.0409(17)	0.0331	0.0518(30)	0.0589(30)	0.0355
δ_K /kHz	[0]	1.39	[0]	0.755	[0]	[0]	0.437
P_a /uÅ^2	294.114181(51)	290.2	463.62244(29)	457.7	706.9643(10)	706.9739(10)	690.6
P_b /uÅ^2	60.834447(51)	60.28	129.66684(29)	126.0	207.5710(10)	207.5653(10)	207.2
P_c /uÅ^2	1.892751(51)	2.32	2.65828(29)	2.767	11.7654(10)	11.7467(10)	9.530
[14]N χ_{aa} /MHz	1.6233(29)	1.74	1.3466(40)	1.40	1.157(63)	1.201(64)	1.16
[14]N χ_{bb} /MHz	2.3948(36)	2.65	2.4335(73)	2.74	2.295(55)	2.320(57)	2.45
[14]N χ_{cc} /MHz	-4.0181(75)	-4.39	-3.780(16)	-4.14	-3.45(11)	-3.52(11)	-3.61
$-(U_p)_z$	-	0.38	-	0.36	-	-	0.28
V_3 /cm^{-1}	373.574(88)	255	385.80(32)	269	404.5(13)	405.6(13)	273
F /GHz	{163.25}[d]	161.9	{160.74}	159.87	{159.94}	{159.97}	159.0
F_0 /GHz	{158.32}	157.6	{158.32}	157.69	{158.32}	{158.32}	157.7
I_α / uÅ^2	{3.192}	3.149	{3.192}	3.205	{3.192}	{3.192}	3.205
ρ	{0.036}	0.0328	{0.017}	0.016	{0.011}	{0.011}	0.009
β /deg	12.360(21)	15.21	16.67(11)	19.96	15.17(50)	14.53(51)	24.26
$\|\mu_a\|$ /D	Yes	1.41	Yes	1.47	Yes	Yes	1.51
$\|\mu_b\|$ /D	Yes	1.03	No	0.61	No	No	0.02
$\|\mu_c\|$ /D	No	0.85	No	0.16	No	No	0.51
N	197/28	-	170/28	-	116/40	119/40	-
σ /kHz	6.9	-	5.8	-	9.6	9.9	-

[a] *A*, *B*, and *C* are the rotational constants. Δ_J, Δ_{JK}, Δ_K, δ_J, and δ_K are the quartic centrifugal distortion constants. P_α (α = *a*, *b*, or *c*) are the planar moments of inertia, these are derived from the moments of inertia I_α as for example $P_c = (I_a+I_b-I_c)/2$. χ_{aa}, χ_{bb}, and χ_{cc} are quadrupole coupling tensor diagonal elements for the ^{14}N atom. $-(U_p)_z$ is the unbalanced *p* orbital occupancy ($-(U_p)_z = -[(n_x+n_y)/2-n_z]$, with *n* being the electron occupancy calculated from NBO analysis). V_3 is the internal rotation barrier for the methyl top. *F* is the reduced internal rotation constant, and F_0 is directly related to the inverse moment of inertia of the methyl top, I_α. ρ is the dimensionless module of the vector **ρ** essential to describe the coupling of internal and overall rotation. β is the angle between the principal inertial axis, *a*, and **ρ**. μ_α (α = *a*, *b*, or *c*) are the electric dipole moment components, Yes or No indicate if *a*-, *b*-, or *c*-type transitions have been observed. *N* is the number of quadrupole hyperfine components/rotational transitions fitted. σ is the rms deviation of the fit. [b] Standard errors in parentheses in units of the last digit. [c] Square brackets denote parameters fixed to 0 in the fit. [d] Curly brackets denote values derived from β and I_α.

As in the monohydrated species, the lines for *syn*-mcb-w$_2$-a also present the splittings due to the internal rotation of the methyl top along with those from the nuclear quadrupole coupling (Figure 2 b)). Finally, another set of weaker lines was observed which could be assigned to a complex between mcb and three molecules of water (*syn*-mcb-w$_3$-a). Under the high-resolution conditions of the Balle-Flygare spectrometers, the lines exhibited a complex splitting structure due to internal rotation, quadrupole coupling and an additional vibrational doubling (Figure 2 c)). The analysis of these spectra was carried out as consisting of transitions in two distinct vibrational states. However, due to the small vibrational splitting, no interacting parameters could be fitted. The sets of experimental parameters are collected in Table 1. The excellent agreement between the experimental and theoretical rotational parameters leads us to conclude that the predicted geometries provide reasonable descriptions of the cluster structures.

For the *syn*-mcb-w-a cluster, several *a*-type and *b*-type transitions with $J \leq 5$ and $K_a \leq 2$ have been observed. Despite the fact that the μ_c dipole moment component is predicted to be of similar magnitude to μ_b (Table 1), no *c*-type transitions have been detected. This is consistent with anticipated flipping (torsional) motion of water around the O-H⋯O bond switching the non-bonded water hydrogen atom from above to below the heavy atom mcb plane. A shallow double minimum potential function with a small barrier at the planar arrangement and the ground vibrational state close to the barrier or above it would lead to an effective zero value of μ_c. In a first approximation, the spectrum was fitted using Pickett´s SPFIT program,[34] which requires that the *A* and *E* states are analyzed independently. The *A* state can be fitted using a standard semirigid, asymmetric rotor Hamiltonian with centrifugal distortion terms using Watson´s *A* reduction[35] in the *I*^{r} representation, augmented with nuclear quadrupole coupling terms.[36] It is also possible to use the SPFIT program to fit the E state transitions. The Hamiltonian is set up with the same terms as those used to analyze the *A* state but adding the parameters, D_a, D_b, and/or D_c which account for the effects of interaction between overall and internal rotation.[37,38] A similar procedure was followed for the *syn*-mcb-w$_2$-a complex, initially fitting the *A* and *E* states independently using SPFIT. For this species, only *a*-type transitions, with *J* up to nine have been detected, in good agreement with the predicted values for the

dipole moment components (Table 1). For the largest cluster, *syn*-mcb-w$_3$-a, the assignment and analysis of the spectrum was complicated by a small doubling only resolvable using the superior resolution of the Balle-Flygare instruments. This additional splitting was attributed to an inversion motion between two equivalent geometries. Similar doublets were observed in the related clusters between three molecules of water and formamide or ethyl carbamate.[10,17] In the formamide⋯(H$_2$O)$_3$ (f-w$_3$) complex a two state Hamiltonian fit including Coriolis terms was possible, resulting in the determination of the energy difference between the two vibrational states, which were labelled as 0 and 1.[10] However, in the case of *syn*-mcb-w$_3$-a the observed lines do not show net non-rigid effects from Coriolis coupling interactions that allow determination of the energy difference between the states. Nevertheless, a two state Hamiltonian was considered for the pair of 0 and 1 levels for the *A* and *E* torsional substates and constructed with the SPFIT program for the *syn*-mcb-w$_3$-a complex. This allows keeping the values of some parameters, such as the centrifugal distortion or quadrupole coupling constants fixed at the same values for the 0 and 1 states reducing the number of necessary determinable parameters. The rotational parameters determined with SPFIT for the three complexes are collected in Tables S4-S8.

An estimate of the barrier height for the internal rotation motion, V_3 could, in principle, be determined from the values of the D_a parameter obtained for the *E* states of all the species.[38] However, in order to determine V_3 directly we analyzed the *A* and *E* states for each species simultaneously by using the XIAM program.[39] Initial values of the methyl top inertial moment I_α, the reduced rotational constant *F*, and the geometrical parameters describing the orientation of the methyl top were calculated from the available structures. The value of the internal rotation barrier V_3, the dimensionless internal rotation vector rho (ρ), and the angle beta (β), between ρ and the principal inertial axis *a*, are the key parameters in the fit.[39,40] In fact the fits required a preliminary calibration step in order to determine which parameters could be reliably fitted. This was possible on the basis of mcb-w-a, which is the only one of the three studied clusters with both *a*- and *b*-type rotational transitions. In this case, the key internal rotation parameters V_3, ρ, β and I_α (equivalent to its inverse F_0) could all be fitted independently.
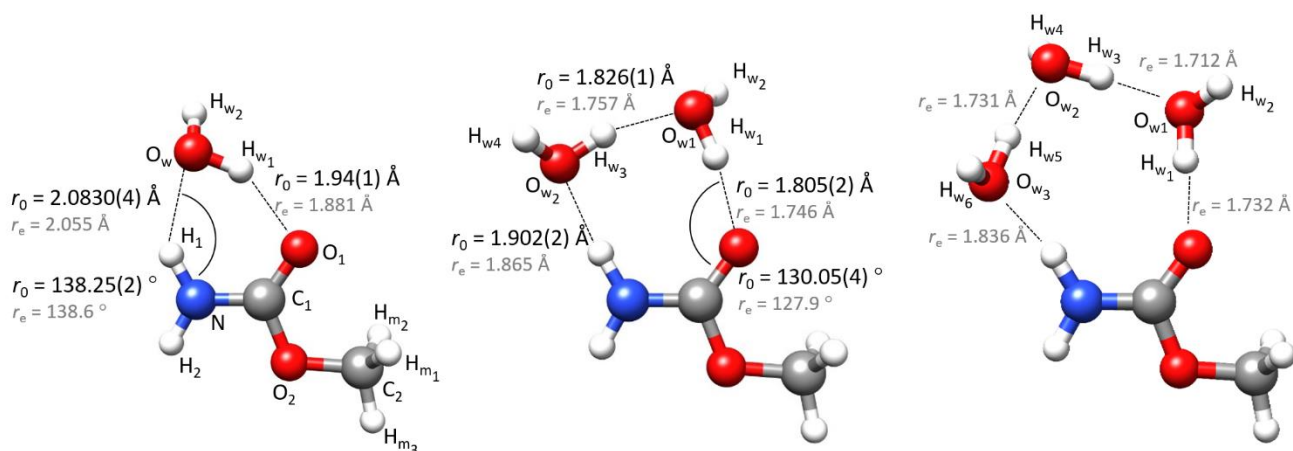
Figure 3. The series of microsolvated clusters of mcb with one, two, or three molecules of water. For the mono and dihydrated complexes, the hydrogen bond parameters determined using the r_0 method are given and compared with the r_e (B3LYP-D3BJ/6-311++G(2d,p)) structure values.

This result is listed in Table S4 and revealed that the fitted methyl top moment $I_\alpha = 3.1921(74)$ uÅ² is practically identical with the computed value of 3.207 uÅ². Furthermore, computations demonstrated invariance of I_α with cluster size. For this reason, it was possible to assume the calibrated value of I_α in fits for all clusters. The stratagem allowed for a pre-calculation of the parameter ρ within XIAM and thus unambiguous determination of V_3 and β for all three hydrated clusters, carried out at the same level of assumptions. Together with the mentioned parameters, rotational and centrifugal distortion constants as well as NQCCs were determined in the fits, as reported in Table 1. Although XIAM allows for the fit of several vibrational states, we decided to make the fits for the 0 and 1 states separately for syn-mcb-w₃-a, since both states were treated as independent also in the SPFIT fit. The results are collected in Tables 1 and S4-S8. A summary of the results obtained for the parent species are given in Table 1. For the $^{18}O_w$ isotopologues for syn-mcb-w-a and syn-mcb-w₂-a we achieved good quality fits using both XIAM and SPFIT (Tables S5 and S7).

The good agreement between the predicted and the determined parameters suggests that the structures for the syn-mcb-w-a, syn-mcb-w₂-a, and syn-mcb-w₃-a clusters are well reproduced by the theoretical calculations. Water closes 6-, 8-, and 10-membered sequential cycles by $C_1=O_1\cdots H_w-O_w$, and $O_w\cdots H_1-N$ hydrogen bonds, respectively (Figure 3). This network is basically identical to the interactions established in similar molecules for 1:1, 1:2 and 1:3 complexes with water.[6,8,11,17] Useful information on the clustered water units is provided by the planar inertial moment P_c, which describes quantitatively the distribution of atomic masses about the ab inertial plane. In the smaller clusters, water locates almost in the mcb plane, as reflected by only a small increase in P_c from the monomer (1.623677(19) uÅ²)[13] to the monohydrated (1.892751(51) uÅ²) and dihydrated cluster (2.65828(29) uÅ²). The P_c values in the $^{18}O_w$ isotopologues (1.89470(11) uÅ² for syn-mcb-w-a, 2.65489(61) uÅ² and 2.6613(11) uÅ² for syn-mcb-w₂-a; Tables S5-S7) further support the near planarity of the heavy atoms in these complexes. For the largest observed cluster, syn-mcb-w₃-a, there is an increase in the P_c value to 11.7654(10) uÅ², arising from the non-planar arrangement of the water moieties. The P_c values for the mcb monomer and its three hydrated complexes are between those for corresponding species involving formamide, with no methyl top, and ethyl carbamate, with an ethyl chain (Table S9). Since vibrational motions together with the out-of-plane hydrogen atoms of the alkyl and water contribute to the planar moments, it is reasonable that the P_c values of mcb are intermediate between those of formamide and ethyl carbamate (Table S9).

Experimental insight into the molecular structure is possible by a least squares fit of some selected structural parameters to the rotational constants for all the available isotopologues.[41] This structure reproduces the rotational constants in the ground vibrational state,[42] and is commonly known as the r_0 structure. The results obtained by this procedure for syn-mcb-w-a, and syn-mcb-w₂-a are shown in Figure 3, and Tables S10-S11, where they are compared with the predicted r_e structure. The coordinates for the ^{18}O atom in the mono substituted isotopologues can be obtained using Kraitchman equations,[43] with uncertainty in the determination estimated according to the Costain rule.[44] The Kraitchman equations give absolute values for the coordinates; therefore, the sign was assigned by comparison with r_0 and r_e structure coordinates. The r_s values are compared with the r_0 and

r_e structure parameters in Table S12 for syn-mcb-w-a and in Table S13 for syn-mcb-w₂-a, demonstrating excellent agreement between the three methods.

Nuclear quadrupole coupling and π-cooperative effects

Resonance Assisted Hydrogen Bonding (RAHB)[45,46] or π-cooperative effects were found to occur in crystal studies of small amides.[47] In the gas phase those effects have also been evidenced recently in the microsolvated complexes of formamide[9,10] and ethyl carbamate.[17] The main effect of cooperativity is an elongation of the C=O and a shortening of the C-N bond with increasing cluster size. If the heavy atom isotopologues are observed, as has been the case of formamide,[9,10] the RAHB effects can be experimentally determined. If no isotopologues are observed, as for ethyl carbamate,[17] or the present case of mcb, then the theoretical bond distances could be used as an approximation (Figure 4).
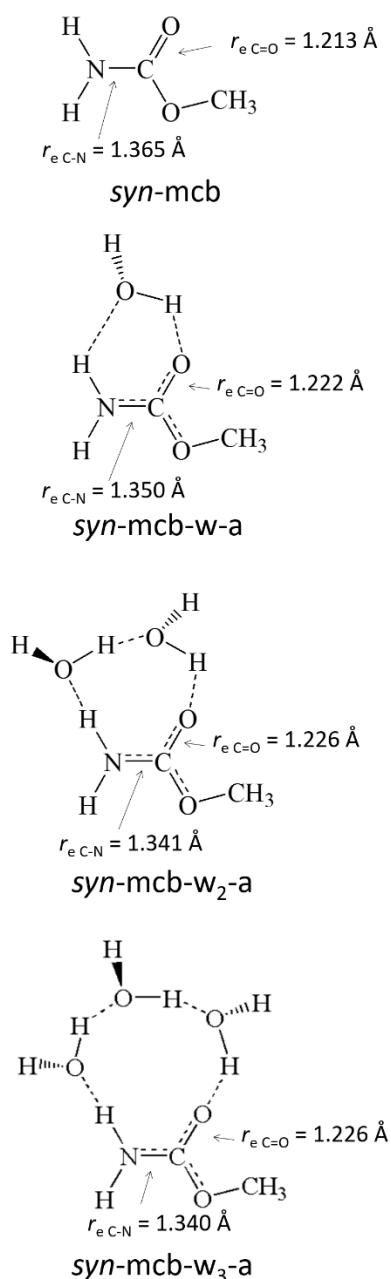

Figure 4. Schematic representation of mcb and its microsolvated complexes illustrating the RAHB effects.
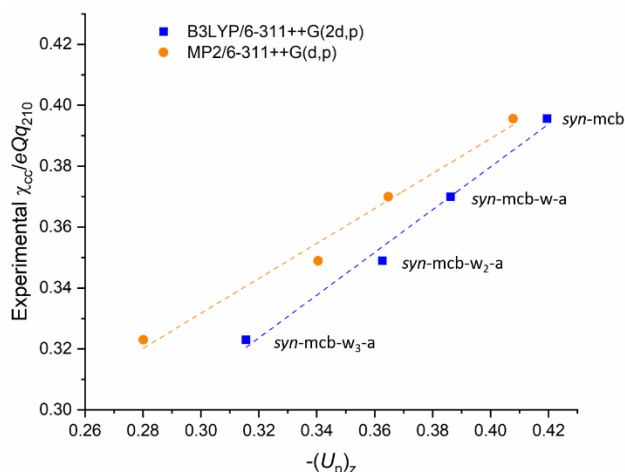
Figure 5. Correlation between experimental χ_{cc} and -$(U_p)_z$ at two levels of theory, B3LYP-D3BJ/6-311++G(2d,p) (blue) and MP2/6-311++G(d,p) (orange). The dashed lines represent the tendency line from a linear fit of the four points.

It has also been demonstrated that NQCCs can be used to identify RAHB or other resonance effects.[9,10,48] The NQCCs are highly sensitive to small changes in the electronic environment of the coupling nucleus, and can be used as a probe to highlight the subtle resonance effects. In principle, it would be necessary to determine the complete nuclear quadrupole coupling tensor. However, in near planar systems, useful information can be extracted even solely from the diagonal elements. For planar or almost planar systems, the c inertial axis is practically perpendicular to the molecular plane, and can be identified with the z axis in the quadrupolar axis system. Thus, the nuclear quadrupole coupling constant perpendicular to the plane in the inertial axis system (χ_{cc}) can be approximated to the constant in the quadrupolar axis system (χ_{zz}), which is directly related to the electronic population and the electric field gradient.[9,36,48]

$$\chi_{zz} = -[(n_x + n_y)/2 - n_z] \cdot eQq_{210}$$

The $-[(n_x + n_y)/2 - n_z]$ term, is usually abbreviated as -$(U_p)_z$ and illustrates the unbalanced electronic charge of the $2p_z$ orbital, which can be obtained from NBO computations.[49] The eQq_{n10} quantity denotes the hypothetical coupling of a single electron in a p orbital in an isolated atom, and for ^{14}N it has been calculated as -10.86(11) MHz.[48]

The small P_c values for the two smaller complexes of mcb highlight their near planarity and validate the use of this approximation. The P_c value for the syn-mcb-w$_3$-a complex shows that it is less planar than the smaller clusters. A similar situation was observed for f-w$_3$[10] and ecb-w$_3$,[17] and the good correlation observed indicates that the approximation is still valid for such clusters, since the N-C=O segment still remains close to the ab inertial plane. Table 1 presents the values of χ_{cc} and -$(U_p)_z$ for the series of microsolvated complexes of mcb reported in this work. The complete theoretical quadrupole coupling tensor at B3LYP-D3BJ/6-311++G(2d,p) and MP2/6-311++G(d,p) levels of theory, the diagonalized tensor, the experimental constants and the calculated -$(U_p)_z$ values are collected in Table S14 in the supplementary material. The experimental χ_{cc} versus -$(U_p)_z$ values are plotted in Figure 5, showing a decreasing tendency with the degree of hydration, in line with results for other systems.[9,10,48] The observed trend in the experimental χ_{cc} values is evidence for the increasing polarization effect of the methyl carbamate molecule with the degree of hydration due to the RAHB. This polarization results in a decrease of the electron density excess along the z-axis (Figure 5 and Table S14).
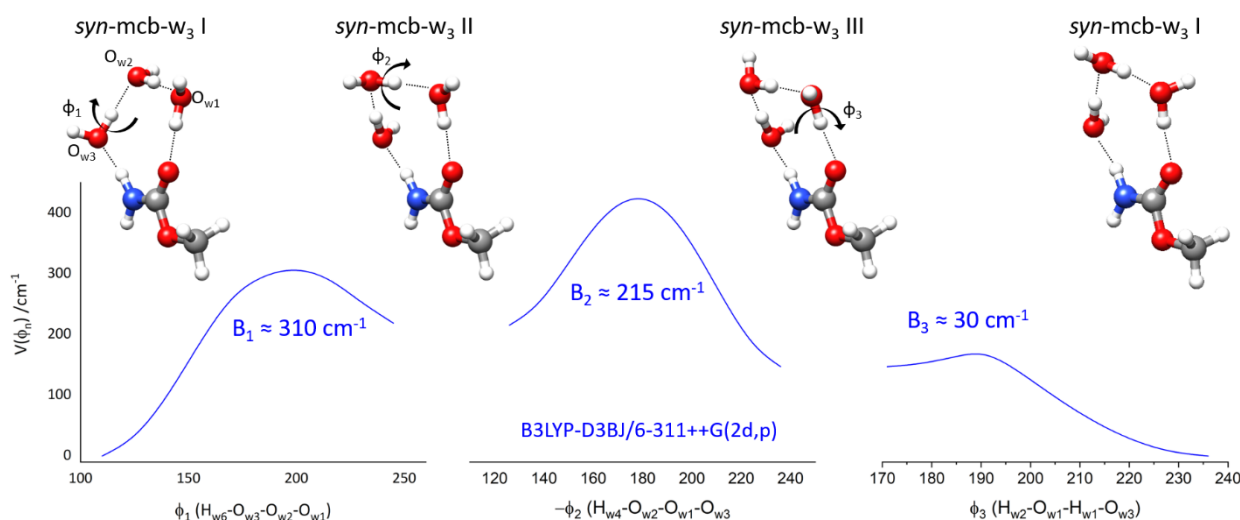

Figure 6. Possible path for the configuration inversion for the trihydrated complex of mcb calculated in three relaxed coordinate scans (B3LYP-D3BJ/6-311++G(2d,p)) by the flipping motion described by the ϕ_1 (H$_{w6}$-O$_{w3}$-O$_{w2}$-O$_{w1}$), ϕ_2 (H$_{w4}$-O$_{w2}$-O$_{w1}$-O$_{w3}$), and ϕ_3 (H$_{w2}$-O$_{w1}$-H$_{w1}$-O$_{w3}$) angles. The barriers for the ϕ_1, ϕ_2, and ϕ_3 scans are represented from left to right, respectively. This path is similar to the one reported for f-w$_3$. Atom is labelling defined in Figure 3.

Large Amplitude Motions and Microsolvation

In discussing the motion which gives rise to the additional splitting in syn-mcb-w$_3$-a, it is reasonable to assume that it follows the same path as that proposed for the clusters of formamide and ethyl carbamate,[10,17] since the structures and hydrogen bond connectivity are similar for all three families of clusters. The suggested path involves a consecutive flipping

motion of each water molecule connecting the three isomers of the complex passing through rather low hindering barriers as shown in Figure 6.

Inspection of the experimental internal rotation barrier values for the monomer and the microsolvated species reveals a steady increasing tendency with the degree of hydration (Table 2). The change from the monomer to the monohydrated clusters is

6

bigger than the changes between successive larger clusters. The theoretical calculations predict the same tendency in the internal rotation barrier, with an upward shift in the absolute values and a minor discrepancy in the step from *syn*-mcb-w$_2$-a to *syn*-mcb-w$_3$-a (Table 2 and Figure 7).

Table 2. Evolution of the experimental and theoretical (B3LYP-D3BJ/6-311++G(2d,p)) internal rotation barrier for *syn*-mcb$\cdots$(H$_2$O)$_n$, n = 0-3 and methyl lactate$\cdots$(H$_2$O)$_n$, n = 0-2. All energies are given in cm^{-1}.

syn-mcb$\cdots$(H$_2$O)$_n$	Experimental V$_3$	Theoretical V$_3$
n = 0	352.18(29)[a]	236
n = 1	373.574(88)	255
n = 2	385.80(32)	269
n = 3	404.5(13)[b]	273

mlc$\cdots$(H$_2$O)$_n$	Experimental V$_3$
n = 0	398.07(25)[c]
n = 1	428(2)[d]
n = 2	433.74(66)[d]

[a] Reference 13. [b] Value for the 0 state. [c] Reference 50. [d] Reference 51.
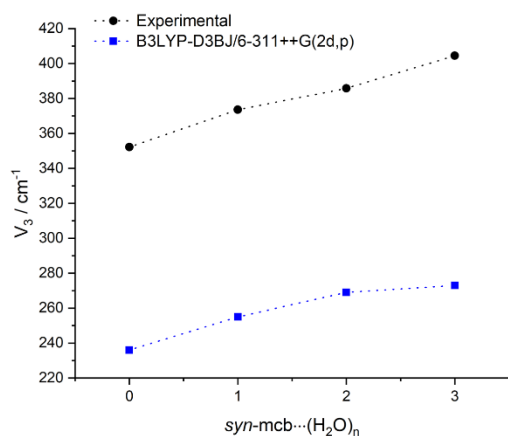
Figure 7. Experimental and theoretical (B3LYP-D3BJ/6-311++G(2d,p)) barrier height for the internal rotation of the methyl top in mcb with increasing hydration degree.

A similar tendency was observed in the series of monomer – monohydrated – dihydrated complexes of methyl lactate (mlc).[50,51] In mlc, the trend in the *V$_3$* value was attributed to the shortening of the O$_1\cdots$H$_{m1}$ and O$_1\cdots$H$_{m2}$ distances, which is also predicted to happen in mcb (Table S15). However, the change in the *V$_3$* barriers for mcb seem to be more pronounced than those of mlc. Changes in the electronic environment of mcb, such as the extension of the resonance and π-cooperative effects to the O$_2$, could also be responsible for the increase in the internal rotation barrier with the degree of hydration.

Conclusions

We have investigated the microsolvated complexes of methyl carbamate using microwave spectroscopy, and determined with high accuracy the rotational constants, the NQCCs, and the barrier heights for the internal rotation motion in three new hydrated mcb clusters. From the parameters of the parent and the single ^{18}O$_w$ isotopologues for the mono- and di-hydrated complexes, we have derived the experimental structures and precisely located the water molecule within the clusters. The heavy atom skeleton of the mono and dihydrated complexes is essentially planar but as in related trihydrate complexes, the water trimer adopts a slightly out-of-plane configuration. The smaller complexes exhibit a splitting in the rotational transitions arising from the internal rotation of the methyl top, as well as a hyperfine structure due to the presence of a ^{14}N nucleus. The complex with three molecules of water presents an additional splitting attributed to an inversion motion resulting in a complicated spectral pattern, which was successfully disentangled. We have observed two interesting trends in the series of microsolvated complexes of methyl carbamate. First, a decrease in the experimental χ_{cc}/eQq_{210} value, correlated with RAHB effects, in line with previous studies of small amides in the gas phase. Secondly, an increase in the experimental V$_3$ barrier, well reproduced by the theoretical calculations. The increase in V$_3$ can be associated with a decrease in the distance between the carbamate oxygen atom and the hydrogen atoms of the rotating top, but may be also influenced by resonance effects. Our study provides insight into the behavior of microsolvated complexes, extending previous research concerning hydration of small amides. The analysis of the complex spectra due to several effects: internal rotation, nuclear quadrupole coupling, and inversion motion is of significant basic interest for molecular spectroscopy since, while these effects are commonly observed, they rarely occur together, as is the case in the *syn*-mcb-w$_3$-a complex.

Author Contributions

Pablo Pinacho: conceptualization, investigation, formal analysis, writing - original draft, writing - review & editing. Juan Carlos López: funding acquisition, project administration, formal analysis, writing - review & editing. Zbigniew Kisiel: investigation, formal analysis, writing - review & editing. Susana Blanco: conceptualization, funding acquisition, project administration, investigation, formal analysis, writing - review & editing.

Conflicts of Interest

Authors declare no conflict of interest.

Supplementary Material

The supplementary material includes Additional figures of conformers, experimentally determined structures and line lists for the observed conformers.

Acknowledgments

Data availability

The data that support the findings of this study can be found in this article, in the supplementary material and from the authors upon reasonable request.

References

[1] D. J. Abraham, D. P. Rotella, *Burger´s medicinal chemistry, drug discovery and development*, 7th edition, Wiley, Hoboken, **2010**.

[2] A. K. Ghosh, M. J. Brindisi, *Med. Chem.*, **2015**, *58*, 2895–2940.

[3] T. R. Fukuto, *Environ. Health Perspect.*, **1990**, *87*, 245–254.

[4] R. H. Heyn, I. Jacobs, R. H. Carr, *Adv. Inorg. Chem.*, **2014**, *66*, 83–115.

[5] C. M. Venkatachalam, *Biopolymers*, **1968**, *6*, 1425–1436.

[6] F. J. Lovas, R. D. Suenram, G. T. Fraser, C. W. Gillies, J. Zozom, *J. Chem. Phys.*, **1988**, *88*, 722–729.

[7] A. Held, D. W. Pratt, *J. Am. Chem. Soc.*, **1993**, *115*, 9708–9717.

[8] S. Blanco, J. C. López, A. Lesarri, J. L. Alonso, *J. Am. Chem. Soc.*, **2006**, *128*, 12111–12121.

[9] S. Blanco, P. Pinacho, J. C. López, *Angew. Chem. Int. Ed.*, **2016**, *128*, 9477–9481.

[10] S. Blanco, P. Pinacho, J. C. López, *J. Phys. Chem. Lett.*, **2017**, *8*, 6060–6066.

[11] P. Pinacho, S. Blanco, J. C. López, *Phys. Chem. Chem. Phys.*, **2019**, *21*, 2177–2185.

[12] R. A. Kydd, A. J. Rauk, *Mol. Struct.*, **1981**, *77*, 227–238.

[13] K. M. Marstokk, H. Møllendal, *Acta Chem. Scan.*, **1999**, *53*, 79–84.

[14] B. Bakri, J. Demaison, I. Kleiner, L. Margulès, H. Mollendal, D. Petitprez, G. Wlodarczak, *J. Mol. Spectrosc.*, **2002**, *215*, 312–316.

[15] P. Groner, M. Winnewisser, R. Medvedev, F. C. De Lucia, E. Herbst, K. V. L. N. Sastry, *ApJS*, **2007**, *169*, 28–36.

[16] V. Ilyushin, E. Alekseev, J. Demaison, I. Kleiner, *J. Mol. Spectrosc.*, **2006**, *240*, 127–132.

[17] P. Pinacho, J. C. López, Z. Kisiel, S. Blanco, *Phys. Chem. Chem. Phys.*, **2020**, *22*, 18351–18360.

[18] P. Pinacho, S. Blanco, Z. Kisiel, J. C. López, *J. Phys. Chem. A*, **2019**, *123*, 7983–7990.

[19] G .G Brown, B. C. Dian, K. O. Douglass, S. M. Geyer, B. H. Pate, *J. Mol. Spectrosc.*, **2006**, *238*, 200–212.

[20] G. G. Brown, B. C. Dian, K. O. Douglass, S. M. Geyer, S. T. Shipman, B. H. Pate, *Rev. Sci. Instrum.*, **2008**, *79*, 053103.

[21] J. L. Alonso, F. J. Lorenzo, J. C. López, A. Lesarri, S. Mata, H. Dreizler, *Chem. Phys.*, **1997***, 218*, 267–275.

[22] Z. Kisiel, J. Kosarzewski, L. Pszczółkowski, *Acta Phys. Pol. A*, **1997**, *92*, 507–516.

[23] A. Kraśnicki, Z. Kisiel, *J. Mol. Spectrosc.*, **2010**, *260*, 57–65.

[24] Gaussian 09, Revision D.01, M. J. Frisch, *et al. Gaussian, Inc., Wallingford CT*, **2016**.

[25] P. Pracht, F. Bohle, S. Grimme, *Phys. Chem. Chem. Phys.*, **2020**, *22*, 7169–7192.

[26] a) C. Lee, W. Yang, R. G. Parr, *Phys. Rev. B*, **1988**, *37*, 785–789. b) A. D. Becke, *J. Chem. Phys.*, **1993**, *98*, 5648–5652.

[27] R. Ditchfield, W. J. Hehre, J. A. Pople, *J. Chem. Phys.*, **1971**, *54*, 724–728.

[28] S. Grimme, J. Antony, S. Ehrlich, H. J. Krieg, *Chem. Phys.*, **2010**, *132*, 154101.

[29] P. Pinacho, J. C. López, S. Blanco, *J. Mol. Spectrosc.*, **2017**, *337*, 145–152.

[30] M. J. Frisch, J. A. Pople, J. S. Binkley, *J. Chem. Phys.,* **1984**, *80*, 3265–3269.

[31] A. D. Becke, E. R. Johnson, *J. Chem. Phys.,* **2005**, *122*, 154101.

[32] C. Møller, M. S. Plesset, *Phys. Rev.*, **1934**, *46*, 618–622.

[33] E. D. Glendening, C. R. Landis, F. Weinhold, *J. Comput. Chem.*, **2013**, *34*, 1429–1437.

[34] H. M. Pickett, *J. Mol. Spectrosc.*, **1991**, *148*, 371–377.

[35] J. K. G. Watson, in *Vibrational Spectra and Structure a Series of Advances, Vol 6* ed. J. R. Durig, Elsevier, New York, **1977**, pp. 1–89.

[36] W. Gordy, R. L. Cook, *Microwave molecular spectra*, Wiley-Interscience, New York, **1972**, vol. 11.

[37] Z. Kisiel, L. Pszczółkowski, E. Białkowska-Jaworska, S. B. Charnley, *J. Mol. Spectrosc.*, **2007**, *241*, 220–229.

[38] D. Gerhard, A. Hellweg, I. Merke, W. Stahl, M. Baudelet, D. Petitprez, G. Wlodarczak, *J. Mol. Spectrosc.*, **2003**, *220*, 234–214.

[39] H. Hartwig, H. Dreizler, *Z. Naturforsch*, **1996**, *51a*, 923–932.

[40] N. Hansen, H. Mader, T. Bruhn, *Molec. Phys.*, **1999**, *97*, 587–595.

[41] Z. Kisiel, *J. Mol. Spectrosc.*, **2003**, *218*, 58–67.

[42] H. D. Rudolph, *Struct. Chem.*, **1991**, *2*, 581–588.

[43] J. Kraitchman, *Am. J. Phys.*, **1953**, *21*, 17–24.

[44] C. C. Costain, *Trans. Am. Crystallogr. Assoc.*, **1966**, *2*, 157–164.

[45] G. A. Jeffrey, *An Introduction to Hydrogen Bonding*; Topics in Physical Chemistry - Oxford University Press, Oxford University Press, **1997**.

[46] P. Gilli, V. Bertolasi, V. Ferretti, G. Gilli, *J. Am. Chem. Soc* **2000**, *122*, 10405–10417.

[47] T. Ottersen, *Acta Chemica Scandinavica*. **1975**, 939–944.

[48] P. Pinacho, D. A. Obenchain, M. Schnell, *J. Chem. Phys.*, **2020**, *153*, 244307.

[49] A. E. Reed, R. B. Weinstock, F. Weinhold, *J. Chem. Phys.* **1985**, *83*, 735–746.

[50] N. Borho, Y. Xu, *Phys. Chem. Chem. Phys.*, **2007**, *9*, 1324–1328.

[51] J. Thomas, O. Sukhorukov, W. Jäger, Y. Xu, *Angew. Chem. Int. Ed.*, **2014**, *53*, 1156–1159.